ICE, CLOUD, and Land Elevation Satellite-2
(ICESat-2) Project

ICESat-2 Data Comparison User's Guide For Release 007

Prepared By:
ICESat-2 Project Science Office

Contributors:
John Robbins,
Tyler Sutterley,
Thomas Neumann,
Nathan Kurtz,
Marco Bagnardi,
Kelly Brunt,
Aimée Gibbons,
David Hancock,
Jeff Lee,
Scott Luthcke

/Code: 615

This document may be cited as:
J. Robbins, T. Sutterley, T. Neumann, N. Kurtz, M. Bagnardi, K. Brunt, A. Gibbons, D. Hancock, J. Lee, and S. Luthcke. *ICESat-2 Data Comparison Guide for Release 007*. ICESat-2 Project, 2025. doi: 10.5281/zenodo.16389971. https://doi.org/10.5281/zenodo.16389971

Goddard Space Flight Center
Greenbelt, Maryland

Release Date: July 2025

Abstract

This document describes methods for making comparisons of Release 007 ICESat-2 data products with results and data from other satellite missions. Included are considerations regarding reference systems, geophysical correction modeling, and underlying assumptions. Transformations are outlined to assist the user community to effectively apply ICESat-2 data in comparisons with independent sources.

Preface

This document provides a guide specifically aimed to assist Release 007 ICESat-2 data users to properly transform ICESat-2 data products into reference systems adopted by other satellite missions, altimetric or otherwise. Initial sections provide step-by-step transformational processes involving reference systems and considerations for geophysical corrections. Later sections provide details on the definitions of various mission reference systems, and discuss underlying assumptions behind modeling choices. A Glossary is provided to aid in gaining an appreciation of geodetic and geophysical correction modeling terminology, used throughout.

The ICESat-2 Project Science Office (PSO) assumes responsibility for this document and updates it, as required, as algorithms are refined or to meet the needs of the ICESat-2 mission. Reviews of this document are performed when appropriate and as needed updates to this document are made. Changes to this document will be made by a complete revision.

Changes to this document require prior approval of the Change Authority listed on the signature page. Proposed changes shall be submitted to the ICESat-2 PSO, along with supportive material justifying the proposed change.

Questions or comments concerning this document should be addressed to:

Tom Neumann, ICESat-2 Project Scientist
Mail Stop 610
Goddard Space Flight Center
Greenbelt, Maryland 20771

Table of Contents

1 Introduction

The ICESat-2 user community possesses very diverse and unique scientific backgrounds, including glaciology, oceanography, atmospheric sciences, hydrology, biogeography and geodesy. There are users with expertise across a whole host of scientific sub-disciplines desiring to compare ICESat-2 data with results and data products from other measurement systems, spaceborne or otherwise. Additionally, there are users interested in quantifying cross-mission instrument and measurement biases.

Appreciating that some of the user community has less exposure to the geodetic underpinnings of the ICESat-2 mission or satellite laser altimetry, this document attempts to provide suggestions and guidance with various transformations and data treatments to assist users in making appropriate comparisons of ICESat-2 results with other satellite mission measurement systems. Other height measurement missions considered include CryoSat-2, the Surface Water and Ocean Topography (SWOT) mission, and the original ICESat mission, herein called ICESat (GLAS). Other missions can be added to later versions of this document, by request of the user community.

Section 2 provides considerations and discussions with regard to height systems, and their relation to the treatment of the permanent tide, critical for inter-comparing mission specific data sources. Section 3 presents primary reference system (ellipsoid) transformations, providing alternatives for making coordinate conversions and ellipsoid transformations. Section 4 provides tables of reference system parameters for each mission. Section 5 provides geophysical correction definitions and parameters adopted for ICESat-2 data products. A Glossary is provided as Appendix A, aiding in formal definitions of geodetic and geophysical terminology used throughout. Illustrations are provided to aid in conceptual understanding.

2 Height Comparisons and Tidal Systems

In this section, some basic concepts are presented in order to facilitate comparisons of ICESat-2 heights with those from other sources or space missions. Clear definitions and distinctions between various tidal systems and their respective treatment of the permanent tide are of utmost importance.

2.1 Tidal Systems

In this context, the term "tidal system," refers to how the *permanent tide* is treated and/or applied to the geoid model and/or for the solid earth tide geophysical correction. Essentially, there are three tidal systems. The discussion, herein, will mainly address two: the *mean tide system* and *tide free system*. A third tidal system is known as the *zero tide system*. For further discussion on tidal systems, see, e.g., Mäkinen and Ihde [2009].

The presence of the Sun and Moon cause a tidal attraction that has periodic and non-periodic components deforming the shape of the geoid (Earth's geopotential) as well as the Earth's crust. The non-periodic, zero frequency, or time-averaged, deformation is termed the permanent tide. The presence of the non-periodic part of the solar and lunar gravitational fields causes the planet's shape to bulge slightly more (increasing the flattening) than the case if the Sun and Moon were "removed" (i.e., set to an infinite distance). An exaggerated profile view of this increased bulge is shown in Figure 2.1. Thus, the permanent tide causes the Earth's shape to be slightly compressed at the poles, and extended in the equatorial plane.

The amount of deformation the geoid and crust endures, due to the permanent tide, is a function of latitude (φ), and two scaling parameters (k_2 and h_2), respectively, known as *Love numbers*.

The *mean tide system* essentially involves anything actually measured in the real world, where the effect of the permanent tide is present. Thus, it is natural to measure, for example, the instantaneous sea level, relative to a reference surface (e.g., the ellipsoid) that implicitly includes deformation caused by the permanent tide.

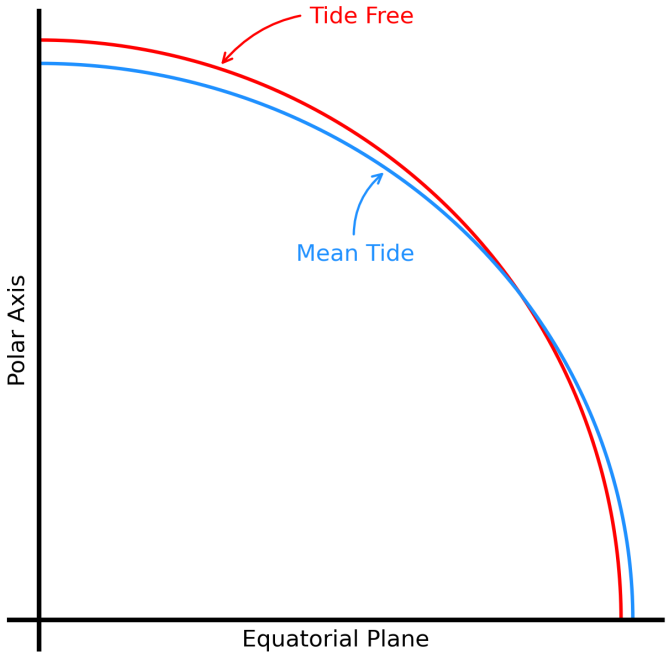

Figure 2.1: Concept of mean tide and tide free systems along a meridian line (not drawn to scale).

The *tide free system* (also known as the non-tidal system) is such that the permanent tide deformation is eliminated from the shape of the Earth, both in terms of a direct (gravitational) and indirect (surface or crustal) response.

2.2 Geoid Considerations for Release 007

Starting with Release 004, the geoid height values are provided in the tide free system. These are transformed into the mean tide system by the equation:

$$\begin{aligned} \texttt{geoid\_free2mean} &= -0.099\ (1.0 + k_2)\ (3.0 \sin^2 \varphi - 1.0) \\ &= 0.1287 - 0.3848 \sin^2 \varphi \end{aligned}$$

Where the degree-2 Love number of gravitational potential, k_2, is set to 0.3 in the lowest equation [Rapp et al., 1991].

The `geoid_free2mean` term is critically important in Release 007 ATL03 and upper-level processing. This term is provided at the same 20m posting as the geoid values. The `geoid_free2mean` term is added to the tide free system geoid height to form a mean tide system geoid height. Combining these steps, for every photon in a 20m along-track interval, the *orthometric height*, relative to the mean tide system is now given as:

$$\begin{aligned} \texttt{h\_ortho} &= \texttt{h\_ph} - \texttt{h\_geoid\_mean} \\ &= \texttt{h\_ph} - (\texttt{h\_geoid} + \texttt{geoid\_free2mean}) \end{aligned}$$

Figure 2.2 illustrates the numerical behavior of the `geoid_free2mean` term, to transform a tide free system geoid height into the mean tide system. It can be seen from the figure that, at the equator, orthometric heights, computed on the basis of the mean tide geoid, will be lower than their corollary, computed on the basis of the tide free geoid. Conversely, at the poles, orthometric heights, computed on the basis of the mean tide geoid,

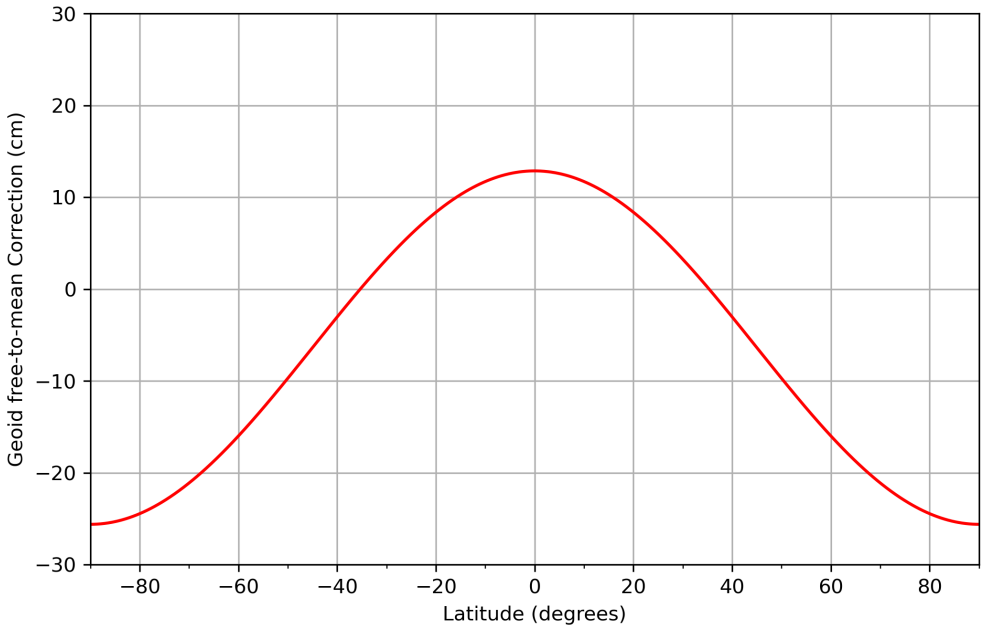

Figure 2.2: Nature of the permanent tide correction for the geoid.

will be higher than their corollary, computed on the basis of the tide free geoid. The permanent tide effect is zero at a latitude of $\pm 35.2644°$. In most cases a mean tide system geoid should be used when re-referencing photon heights from the ellipsoid to the geoid.

2.3 Solid Earth Tide Considerations for Release 007

Similar to the geoid, the solid earth tides can be provided in a tide free system or in a mean tide system. Tide free system solid earth tides include the permanent tide as they realize tide free elevations when subtracted from the observed elevations. On ATL03, from Release 001 onwards, the solid earth tides have been computed in a tide free system. The ATL03 algorithm directs that the solid earth tides (among other geophysical corrections, c.f., Neumann et al. [2019]) be applied to the initial (i.e., uncorrected, or raw) photon heights. Thus, the photon heights, `h_ph`, found on the ATL03 product (and used as input by upper-level products), are ellipsoid heights in a tide free system having been corrected for the effect of the tide free system, solid earth tides.

This situation is especially useful for direct comparisons with ground-based, GNSS and GPS measurements, where heights are typically provided in a tide free system.

However, there may be occasions when users will prefer to work with heights relative to the ellipsoid, given in terms of the mean tide system (e.g., in comparisons with tide gauge, or other satellite altimetry data). In the case when the photon height, relative to the WGS84 ellipsoid (not to the EGM2008 geoid), is required to be in the mean tide system, the following equation is applicable:

$$\begin{aligned} \texttt{tide\_earth\_free2mean} &= -0.09922\, h_2\, (3.0 \sin^2 \varphi - 1.0) \\ &= 0.06029 - 0.180873 \sin^2 \varphi \end{aligned}$$

Where the degree-2 Love number of vertical deformation, h_2, is set to 0.609 in the lowest equation [Rapp et al., 1991]. The above equation is applicable when it is desired to transform earth tide values from tide free to mean tide systems. For Release 004 and subsequent releases, values based on this equation are provided

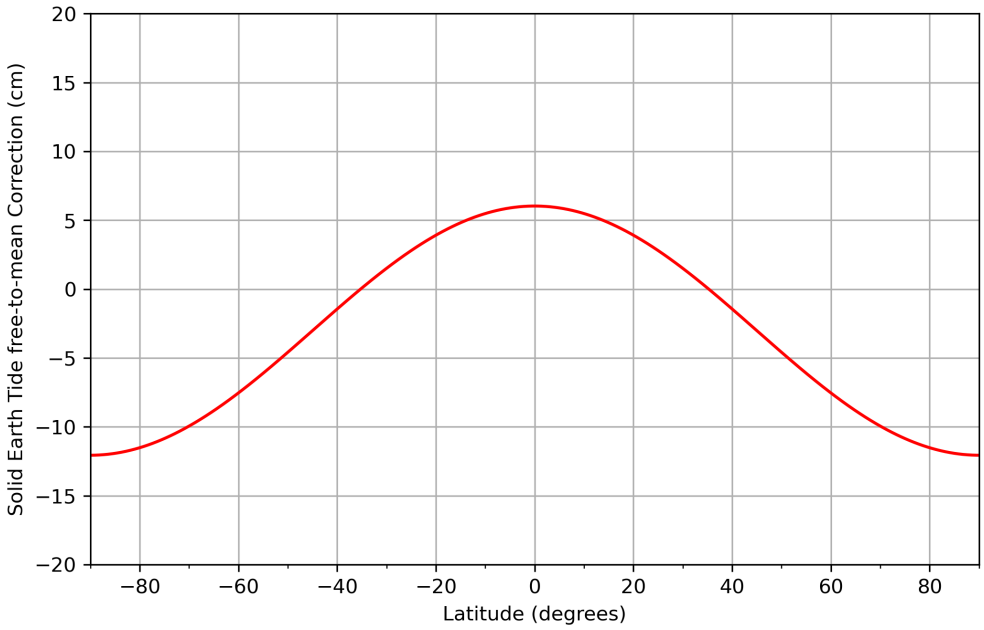

Figure 2.3: Nature of the permanent tide correction for the solid earth tides.

on ATL03 (and upper-level products). For Release 001 through Release 003, the user must compute this term and apply it when appropriate. The ATL03 parameter is called `tide_earth_free2mean`, also located in the `gtx/geophys_corr` group, at the 20m posting. When needed and appropriate, this term is *subtracted* from the tide free system solid earth tide value in order to form a mean tide system solid earth tide. Mean tide system solid earth tides do not include the permanent tide as they realize mean tide elevations when subtracted from observed elevations.

Figure 2.3 shows the `tide_earth_free2mean` term, which can transform a tide free system solid earth tide value into the mean tide system. From the figure, the following can be inferred: the solid earth tide at the equator that realizes a tide free system will be greater than the value that realizes a mean tide system; conversely, the solid earth tide at the poles in the free tide system will be less than the mean tide system value. Again, at latitudes $\pm 35.2644°$, the permanent tide effect is zero.

Application: To transform an ATL03 photon ellipsoid height (`h_ph`) to refer to the mean tide system solid earth tide, this equation is used:

$$\texttt{h\_ph\_mean} = \texttt{h\_ph} + \texttt{tide\_earth\_free2mean}$$

In this case, an addition is made since ATL03's `h_ph` parameter, by default, has the tide free system solid earth tide correction applied. In other words, given that $\texttt{h\_ph} = \texttt{h\_ph\_raw} - \texttt{tide\_earth}$, where `h_ph_raw` is the photon height relative to the ellipsoid without any solid earth tide applied, and where `tide_earth` is defined as being in the tide free system, then, with $\texttt{tide\_earth\_mean} = \texttt{tide\_earth} - \texttt{tide\_earth\_free2mean}$, we get

$$\begin{aligned}\texttt{h\_ph\_mean} &= \texttt{h\_ph\_raw} - (\texttt{tide\_earth} - \texttt{tide\_earth\_free2mean}) \\ &= (\texttt{h\_ph\_raw} - \texttt{tide\_earth}) + \texttt{tide\_earth\_free2mean} \\ &= \texttt{h\_ph} + \texttt{tide\_earth\_free2mean}\end{aligned}$$

3 Geodetic Transformations

This section provides instructions on how to transform ICESat-2 height products from their adopted reference system into reference systems adopted by other missions. Definitions of fundamental reference system parameters are given in Section 4. The glossary provides assistance in clearly defining the technical terminology adopted here, shown in italics.

The main consideration of this section is to describe methods required to transform heights and latitudes, that are given relative to various surfaces. The foundational surface is that of an ellipsoid of revolution that mathematically approximates the shape of the Earth. An important secondary surface is mean sea level, approximated by the geoid, which, itself, is an equipotential surface.

These two primary height reference surfaces are typically specified by each altimetric mission, and are tabulated in Section 4.

3.1 Transformations Between Reference Ellipsoids

All altimetric missions utilize ellipsoids centered at the center of mass of the Earth, and oriented along the same axes (*geocentric*). The problem can be stated as such: Given geodetic coordinates in one ellipsoidal system (A), it is desired to transform them into another ellipsoidal system (B).

$$(\varphi, \lambda, h)_A \rightarrow_T (\varphi, \lambda, h)_B$$

Translations and rotations between ellipsoids and datums are not considered here. Specific realizations of the International Terrestrial Reference Frame (ITRF) may need consideration, by the user (cf., Section 3.2).

There are several ways to make transformations between geocentric ellipsoidal reference systems. Two methods are described, here. The first way is to apply a two-step conversion, where one first converts geodetic coordinates (φ, λ, h) into Cartesian coordinates (X, Y, Z) using the parameters from the first ellipsoid (semi-major axis, a, and the inverse flattening, $1/f$); then make an inverse conversion, from Cartesian (X, Y, Z) back into geodetic coordinates (φ, λ, h), using the parameters from the second ellipsoid. A second way to make the transformation is to use a differential **projective transformation procedure**.

Additionally, there are software procedures freely available that facilitate making these kinds of coordinate conversions and transformations. For example, the Generic Mapping Tools (`GMT`) is able to make ellipsoid transformations within the command, `mapproject`. Within the Matlab environment, a very useful package, called Geodetic Transformations (by Peter Wasmeier) is available from Matlab's file exchange. Within the Python environment, `pyproj` and `geopandas` both provide useful interfaces to `PROJ` transformations (see pipelines in Appendix C).

3.1.1 Two-Step Conversion

This process involves two steps of coordinate conversion, involving the computation of, and utilization of an intermediate set of three-dimensional, Cartesian coordinates:

$$(\varphi, \lambda, h)_A \rightarrow_T (X, Y, Z) \rightarrow_T (\varphi, \lambda, h)_B$$

This begins by computing the radius of curvature in the prime vertical, N, (i.e., perpendicular to the local meridian) for the specific location, using the ellipsoid parameters $(a, f)_A$ for which the geodetic coordinates (φ, λ, h) exist (for ellipsoid A),

$$N = \frac{a}{\sqrt{1 - e^2 \sin^2 \varphi}}$$

Where, e^2 is the square of the first eccentricity, $e^2 = {}^{(a^2-b^2)}/_{a^2} = 1-(1-f)^2$. Then, the 3D-space Cartesian coordinates can be computed via (click here for an online tool):

$$\begin{bmatrix} X \\ Y \\ Z \end{bmatrix} = \begin{bmatrix} (N+h)\cos\varphi\cos\lambda \\ (N+h)\cos\varphi\sin\lambda \\ \left(\left(1-e^2\right)N+h\right)\sin\varphi \end{bmatrix}$$

Once the Cartesian coordinates are computed, then, using the parameters for the ellipsoid B, $(a, f)_B$, the inverse transformation is applied. This is trivial for the longitude, as $\tan\lambda = {}^{Y}/_{X}$, which, since the origin and orientation are common between the two ellipsoids, the longitude for the second ellipsoid will be the same as the longitude for the first.

Computing the latitude (φ) and height (h) is often done in an iterative way, but can also be done in a nearly direct way. One such method is outlined here (Vermeille's method). An online Cartesian to Geodetic tool can be accessed here (not all ellipsoids are represented).

The method computes a set of intermediate parameters, using parameters that pertain to the ellipsoid B;

$$p = \frac{X^2+Y^2}{a^2}$$

$$q = \frac{1-e^2}{a^2}Z^2$$

$$r = \frac{p+q-e^4}{6}$$

$$s = e^4\frac{pq}{4r^3}$$

$$t = \sqrt[3]{1+s+\sqrt{s(2+s)}}$$

$$u = r\left(1+t+\frac{1}{t}\right)$$

$$v = \sqrt{u^2+e^4q}$$

$$w = e^2\frac{u+v-q}{2v}$$

$$k = \sqrt{u+v+w^2}-w$$

$$D = \frac{k\sqrt{X^2+Y^2}}{k+e^2}$$

Then, geodetic latitude and height above the ellipsoid is given by,

$$\varphi = 2\tan^{-1}\left(\frac{Z}{D+\sqrt{D^2+Z^2}}\right)$$

$$h = \frac{k+e^2-1}{k}\sqrt{D^2+Z^2}$$

3.1.2 Differential Projective Transformation

The differential projective transformation procedure computes changes to latitude and height as a function of the change in semi-major axis ($da = a_B - a_A$) and the change in flattening ($df = f_B - f_A$), utilizing the ellipsoid parameters from ellipsoid A. The resulting change in latitude ($d\varphi$) and height (dh) are applied to the coordinates $(\varphi, h)_A$ to yield $(\varphi, h)_B$.

$$(\varphi, h)_A \rightarrow_{T[f(da,df)]} (d\varphi, dh)$$
$$\varphi_B = \varphi_A + d\varphi$$
$$h_B = h_A + dh$$

$$d\varphi = \frac{1}{M+h}\left[\frac{e^2 \sin\varphi\cos\varphi}{W} + \sin\varphi\cos\varphi\left(2N + e'^2 M \sin^2\varphi\right)(1-f)\,df\right]$$

$$dh = -W\,da + \frac{a(1-f)}{W}\sin^2\varphi\,df$$

Where $W = \sqrt{1 - e^2\sin^2\varphi}$, $M = {}^{a(1-e^2)}/_{W^3}$ (the radius of curvature in the meridian), $N = {}^{A}/_{W}$ (the radius of curvature in the prime vertical, perpendicular to the prime meridian) and $e'^2 = {}^{a^2-b^2}/_{b^2}$ (the square of the second eccentricity).

3.1.3 Example of Ellipsoid Transformation

As a numerical example, given geodetic coordinates in the WGS84 ellipsoid system (such as ICESat-2 geolocated photons), and we wish to transform these into the TOPEX/Poseidon (T/P), ellipsoid system (such as ICESat (GLAS) surface elevations) [ITRF considerations are described in Section 3.2].

Given these example geodetic coordinates, in WGS84:

$$\begin{bmatrix}\varphi\\ \lambda\\ h\end{bmatrix}_{WGS84} = \begin{bmatrix}47.0^\circ\\ 15.0^\circ\\ 1200.0\text{ m}\end{bmatrix}$$

Using the **two step method**: first convert the WGS84 geodetic coordinates into Earth-centered Cartesian coordinates (units: meters):

$$\begin{bmatrix}X\\ Y\\ Z\end{bmatrix} = \begin{bmatrix}4209993.6131\\ 1128064.3888\\ 4642642.4133\end{bmatrix}$$

Next, applying the inverse conversion, utilizing the T/P ellipsoid parameters, we compute new latitude, longitude and height to be:

$$\begin{bmatrix}\varphi\\ \lambda\\ h\end{bmatrix}_{T/P} = \begin{bmatrix}47.000000123^\circ\\ 15.000000000^\circ\\ 1200.7073059\text{ m}\end{bmatrix}$$

The **differential projective transformation** starts with WGS84 coordinates, above, utilizing the ellipsoidal difference quantities, $da = -0.7$m and $df = 0.00000000251315$, we compute

$$\begin{bmatrix}d\varphi\\ dh\end{bmatrix} = \begin{bmatrix}0.000000123^\circ\\ 0.7073059\text{ m}\end{bmatrix}$$

thus yielding the same result as the two step method when $d\varphi$ and dh are added to the original WGS84 latitude and height.

3.2 Mission Specific Ellipsoid Transformations

This section provides information needed for transforming coordinates adopted by one mission into coordinates adopted by the ICESat-2 mission. In these cases, adoption of International Terrestrial Reference Frame (ITRF) definitions becomes important when making transformations. For the first 6 releases of the along-track data, the ICESat-2 mission was set in the ITRF2014 realization. With Release 007, the ICESat-2 mission consistently adopted the ITRF2020 realization. The ITRF transformations (Helmert parameters) from ITRF2020 to earlier realizations of the ITRF are given in Appendix B.

3.2.1 Between ICESat-2 and CryoSat-2

Both CryoSat-2 and ICESat-2 adopt the WGS84 ellipsoid as their reference ellipsoid. But, as of Release 007, they no longer are placed in the same realization of the ITRF, since CryoSat-2 remains in the ITRF2014 system. While no transformation for the ellipsoid is required, a slight set of Cartesian translation parameters are required to place the data in the same reference frame (1 to 2 mm in translation and sub ppb scale factor).

ITRF Considerations: Given that the CryoSat-2 data is geolocated within ITRF2014, the coordinates require an additional translation to bring them into ICESat-2's ITRF2020 framework.

Equation 1 of Appendix B is reversed to transform CryoSat-2 ITRF2014 (XS, YS, ZS) coordinates into the ICESat-2 ITRF2020 frame (X, Y, Z).

$$\begin{bmatrix} X \\ Y \\ Z \end{bmatrix} = \begin{bmatrix} XS \\ YS \\ ZS \end{bmatrix} - \begin{bmatrix} T_x \\ T_y \\ T_z \end{bmatrix} - \begin{bmatrix} D & -R_z & R_y \\ R_z & D & -R_x \\ -R_y & R_x & D \end{bmatrix} \begin{bmatrix} XS \\ YS \\ ZS \end{bmatrix}$$

Use of this equation is made with Cartesian form of the coordinates. Coordinate transformations needed to convert from geodetic to Cartesian, and back again, were described in Section 3.1.1.

In this specific case (ITRF2014 to ITRF2020), no rotations are involved, and the above equation, reduces to

$$\begin{bmatrix} X \\ Y \\ Z \end{bmatrix} = \begin{bmatrix} XS \\ YS \\ ZS \end{bmatrix} - \begin{bmatrix} T_x \\ T_y \\ T_z \end{bmatrix} - D \begin{bmatrix} XS \\ YS \\ ZS \end{bmatrix}$$

3.2.2 Between ICESat-2 and SWOT

Similar to ICESat-2, the NASA Surface Water and Ocean Topography (SWOT) mission also adopts the WGS84 ellipsoid as its reference ellipsoid. However as of this writing, data from the SWOT mission are available in the ITRF2014 realization, with plans to transition to ITRF2020 in a future release. Comparing ICESat-2 data with SWOT data requires use of the transformations described in Section 3.2.1.

3.2.3 Between ICESat (GLAS) and ICESat-2

The reference systems adopted by each mission differ in two main ways. First, their respective ellipsoid parameters differ; and second, the coordinate frame for each mission are given across two different realizations of the ITRF. ITRF-2008 was the final adopted terrestrial reference frame for ICESat (GLAS) [Schutz and Urban, 2014, Appendix B]. The latest release (Release-34) of ICESat (GLAS) data is given in the ITRF2008 realization.

Ellipsoid Parameters: ICESat (GLAS) adopted the TOPEX/Poseidon (T/P) ellipsoid (cf., Table 4.1 in Section 4 for parameters) which is an ellipsoid that can fit wholly inside the WGS84 ellipsoid (Figure 3.1). In other words, the T/P ellipsoid is ~70cm smaller than WGS84. Generally, without consideration of ITRF translations and rotations, heights above the T/P ellipsoid will be 70 to 71.37cm larger than WGS84 ellipsoidal heights for the same point (P) in three-dimensional space (as seen in the example, below).

ITRF Considerations: Given that the ICESat (GLAS) data is geolocated within ITRF2008, then coordinates require an additional translation to bring them into ICESat-2's ITRF2020 framework.

Equation 1 of Appendix B is reversed to transform ICESat (GLAS) ITRF2008 (XS, YS, ZS) coordinates into the ICESat-2 ITRF2020 frame (X, Y, Z).

$$\begin{bmatrix} X \\ Y \\ Z \end{bmatrix} = \begin{bmatrix} XS \\ YS \\ ZS \end{bmatrix} - \begin{bmatrix} T_x \\ T_y \\ T_z \end{bmatrix} - \begin{bmatrix} D & -R_z & R_y \\ R_z & D & -R_x \\ -R_y & R_x & D \end{bmatrix} \begin{bmatrix} XS \\ YS \\ ZS \end{bmatrix}$$

Use of this equation is made with Cartesian form of the coordinates. Coordinate transformations needed to convert from geodetic to Cartesian, and back again, were described in Section 3.2.1. In this specific case (ITRF2008 to ITRF2020), no rotations are involved, and the above equation, reduces to

$$\begin{bmatrix} X \\ Y \\ Z \end{bmatrix} = \begin{bmatrix} XS \\ YS \\ ZS \end{bmatrix} - \begin{bmatrix} T_x \\ T_y \\ T_z \end{bmatrix} - D \begin{bmatrix} XS \\ YS \\ ZS \end{bmatrix}$$

Example: In this example, let's say we are given an ICESat (GLAS) geolocated observation, that refers to the TOPEX/Poseidon ellipsoid, in the ITRF2008 frame with an observational epoch of 2005.3 of:

$$\begin{bmatrix} \varphi \\ \lambda \\ h \end{bmatrix}_{T/P,\ ITRF2008,\ 2005.3} = \begin{bmatrix} 42.0^\circ \\ 10.0^\circ \\ 210.0\ \text{m} \end{bmatrix}$$

The first step is to convert these coordinates into Earth-centered fixed Cartesian form using Section 3.1.1 and the parameters for the TOPEX/Poseidon ellipsoid (Table 4.1), yielding (in meters):

$$\begin{bmatrix} X \\ Y \\ Z \end{bmatrix} = \begin{bmatrix} 4675034.5692 \\ 824334.7303 \\ 4245743.8709 \end{bmatrix}$$

Next, the values of the scale, D, and translations, (Tx, Ty, Tz), are adjusted to place them into the 2005.3 epoch (values obtained from Appendix B);

$$\begin{aligned} D_{2005.3} &= D_{2015} + \dot{D}(2005.3 - 2015) \\ &= -0.29 + 0.03(-9.7) \\ &= -0.581\text{ppb} \end{aligned}$$

$$\begin{aligned} \begin{bmatrix} T_X \\ T_Y \\ T_Z \end{bmatrix}_{2005.3} &= \begin{bmatrix} T_X \\ T_Y \\ T_Z \end{bmatrix}_{2015} + (2005.3 - 2015) \begin{bmatrix} \dot{T}_X \\ \dot{T}_Y \\ \dot{T}_Z \end{bmatrix} \\ &= \begin{bmatrix} 0.2 \\ 1.0 \\ 3.3 \end{bmatrix}_{2015} + (-9.7) \begin{bmatrix} 0.0 \\ -0.1 \\ 0.1 \end{bmatrix} = \begin{bmatrix} 0.2 \\ 1.97 \\ 2.33 \end{bmatrix} \text{mm} \end{aligned}$$

Applying the transformation, from ITRF2008, epoch 2005.3 to ITRF2020, epoch 2015 yields:

$$\begin{bmatrix}4675034.5692\\824334.7303\\4245743.8709\end{bmatrix} - \begin{bmatrix}0.0002\\0.00197\\0.00233\end{bmatrix} - (-0.581 \times 10^{-9}) \begin{bmatrix}4675034.5692\\824334.7303\\4245743.8709\end{bmatrix} = \begin{bmatrix}4675034.5692\\824334.7303\\4245743.8709\end{bmatrix} - \begin{bmatrix}-0.0025\\0.0015\\-0.0001\end{bmatrix}$$

$$= \begin{bmatrix}4675034.5717\\824334.7288\\4245743.8711\end{bmatrix}$$

Converting Earth-centered fixed Cartesian coordinates back into WGS84 geodetic coordinates, in the ITRF2020 (2015 epoch) reference system, yields:

$$\begin{bmatrix}\varphi\\\lambda\\h\end{bmatrix}_{WGS84,\ ITRF2020,\ 2015} = \begin{bmatrix}41^\circ\ 59'\ 59.9999''\\9^\circ\ 59'\ 59.9995''\\209.2956\ \mathrm{m}\end{bmatrix}$$

Examining the two sets of coordinates (transformed and un-transformed), it can be seen that the latitude and longitude changed less than one milli-arcsecond, but the transformed height is now 0.704m lower than original un-transformed value. This is expected, given that the surface of the WGS84 ellipsoid is between 70 and 71.37 cm above that of the TOPEX/Poseidon ellipsoid (Figure 3.1). In this particular example, the ITRF transformation (to epoch 2015) only amounted to translations of 1.6mm to 5.7mm.

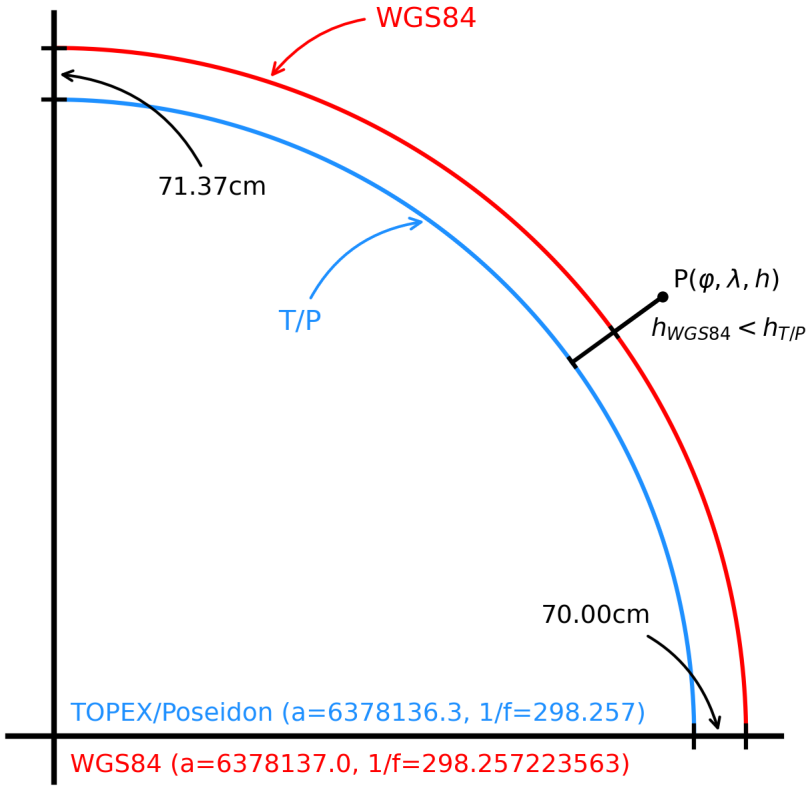

Figure 3.1: Difference between the TOPEX/Poseidon (T/P) ellipsoid (in blue) used with ICESat (GLAS), and WGS84 ellipsoid (in red) used with ICESat-2 (not drawn to scale).

4 Reference Systems & Geoids

The tables (4.1 and 4.2) in this section provide the fundamental values associated with the reference system adopted by various satellite missions.

Table 4.1 provides the mission ellipsoid specification. The ellipsoid is a mathematical definition, as a surface of revolution closely fitting the actual shape of the Earth. The semi-major axis is an approximate radius of the Earth in the equatorial plane. The flattening describes the degree of oblateness.

Table 4.1: Ellipsoid specifications by mission

Mission	Ellipsoid Name	Semi-major Axis (m)	Flattening
ICESat-2	WGS84	6,378,137.0	1/298.257223563
SWOT	WGS84	6,378,137.0	1/298.257223563
ICESat (GLAS)	TOPEX/Poseidon	6,378,136.3	1/298.257
CryoSat-2	WGS84	6,378,137.0	1/298.257223563

Other auxiliary parameters can be computed from these values [Hofmann-Wellenhof and Moritz, 2006]. For example, the semi-minor (polar) axis for WGS84 is given by,

$$b = a\,(1 - f) = 6378137\left(1 - \frac{1}{298.257223563}\right) = 6356752.3142\text{m}$$

And the square of the first eccentricity is given by,

$$e^2 = 1 - (1 - f)^2 = 0.00669437999$$

Table 4.2 provides geoid specification by mission. The geoid is a level surface, or equipotential surface that represents the actual shape of the planet, neglecting topography/bathymetry.

Table 4.2: Geoid specifications by mission

Mission	Geoid Name	Tidal System	Maximum Degree
ICESat-2	EGM2008	Tide Free	2190
SWOT	EGM2008	Mean Tide	2190
ICESat (GLAS)	EGM2008	Mean Tide	2190
CryoSat-2 (ice processor)	EGM96	–	360
CryoSat-2 (ocean processor)	EGM2008	Mean Tide	2190

The mean tide system means that the geoid heights include the effect of the geoid deformation due to the permanent (time-invariant) tide, caused by the gravitational pull from the Moon and Sun. The tide free system does not include the permanent tide. See Section 2.2 for special considerations regarding the utilization of ICESat-2's geoid as a reference surface (e.g., to approximate mean sea level).

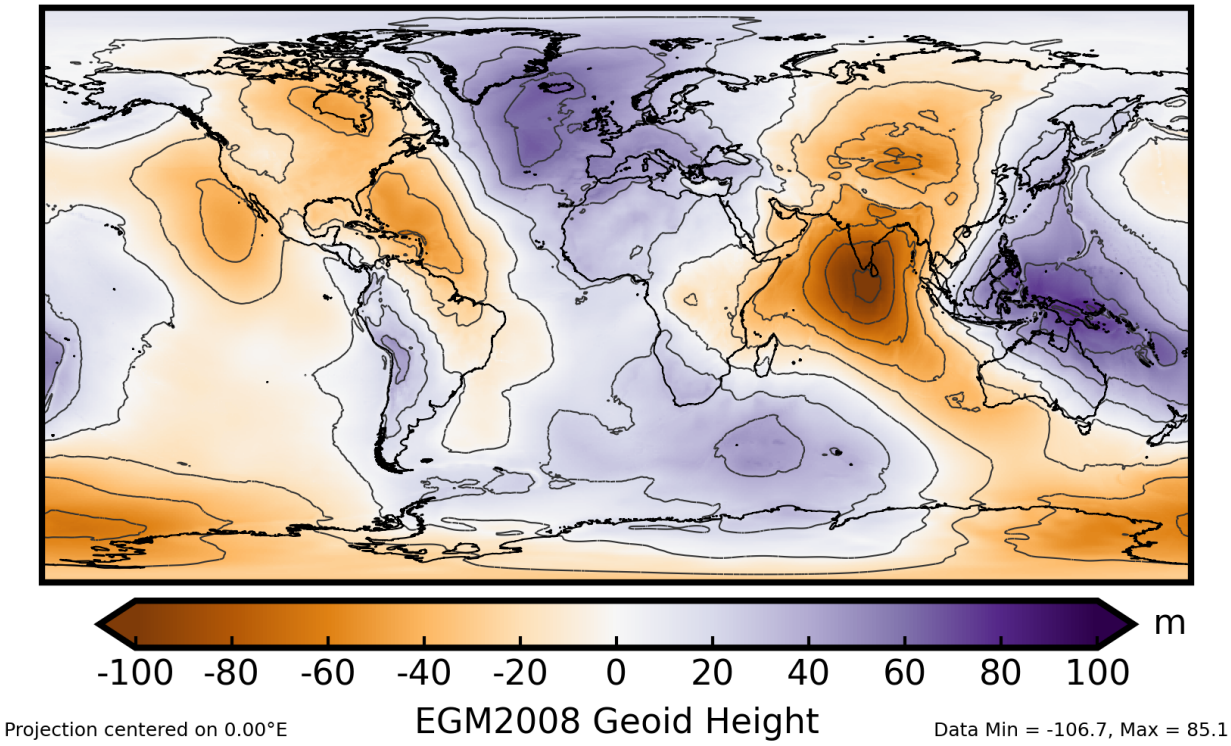

Figure 4.1: EGM2008 geoid heights, relative to the WGS84 ellipsoid. Notable are the Indian low, the East Indies high and the North Atlantic high.

As mentioned above, the ellipsoid is an approximate mathematical description of the shape of the planet. The geoid provides an even better representation of the sea level surface. The global variations in the EGM2008 geoid are shown in Figure 4.1. These variations are due to variations in the distribution of planetary mass at depth. It is worth noting that on ATL03, photon heights are given relative to the WGS84 ellipsoid. This means that photon heights for locations at or near sea level can be negative (less than zero).

5 Considerations For Geophysical Corrections

Satellite altimetry operates on the principle of measuring a round-trip travel time traversed by a signal (laser or radar) emitted from a satellite at altitude, reflected by a real-world surface, and detected by receiver systems on-board the satellite. The determination of a height, at the reflection point on the planetary surface, must be understood as a range from the observation platform (satellite or airborne) to an instantaneous, typically dynamic, surface. For ICESat-2, reflective surfaces can include oceans, inland water bodies, solid ground, land and sea ice, vegetation and man-made structures.

Figure 5.1 provides a conceptual schematic to illustrate the various reference systems (covered in Sections 2 through 4) and dynamic processes that take place at the time when a range measurement is observed by ICESat-2. For example, in order to yield an estimate of the mean sea surface from ICESat-2 data, a number of well-modeled, time-varying effects must be accounted for and removed. This section describes these effects and how they are represented, and/or applied on the ATL03 product. Upper level products may apply more of these corrections in a selective fashion. Additional detail can be found in the Algorithm Theoretical Basis Documents (ATBDs) of the higher-level ICESat-2 products.

Generally, an instantaneous surface height, H (or, in ATL03 terms, a photon event height (h_ph), cf., Neumann et al. [2019]), is defined as follows:

$$H = H^{sat}_{ellipsoid} - H^{sat}_{surface}$$

where $H^{sat}_{ellipsoid}$ is the distance to the satellite above the ellipsoid (determined by precision orbit determination); and is $H^{sat}_{surface}$ the re-tracked range (i.e., the actual measurement, corrected for atmospheric range effects). Next, the photon event height, H, is corrected for an i-number of temporally and spatially varying geophysical effects (tides, loading, etc., as listed below in Table 5.1), that are represented by C_i, which are, by convention, consistently subtracted via:

$$H_{gc} = H - \sum_i C_i$$

where H_{gc} are geophysically-corrected photon event heights, referring to the WGS84 ellipsoid. These geophysically-corrected photon event heights are the `gtx/heights/h_ph` values on the ATL03 data product.

The geophysical corrections necessary over each surface-type are given in Table 5.1. Since some of the corrections are applicable across all surface types, they are applied within ATL03, at the photon height level. These include: ocean loading; solid earth pole tides; ocean pole tides; and solid earth tides. The total column atmospheric range-delay term is also applied within ATL03, but is not discussed here.

Table 5.1: Geophysical corrections as applied by surface type.

Surface Type or Application	Geophysical Corrections Applied
Geolocated Photons (ATL03)	Ocean loading (Section 5.2) Solid Earth tide (Section 5.3) Solid Earth & ocean pole tide (Section 5.4)
Land Ice (ATL06/11)	No additional corrections
Sea Ice (ATL07/10)	Referenced to Mean Sea Surface (see Kwok and Morison [2016]) Ocean tide (Section 5.1) Long period equilibrium ocean tide (Section 5.1) Dynamic Atmospheric Correction (IB + wind effects, Section 5.5)
Land/Vegetation (ATL08)	No additional corrections
Ocean (ATL12)	Ocean tide (Section 5.1) Long period equilibrium ocean tide (Section 5.1) Dynamic Atmospheric Correction (IB + wind effects, Section 5.5)
Inland Water (ATL13)	No additional corrections
Coastal Bathymetry (ATL24)	Referenced to geoid surface (Section 2.2)

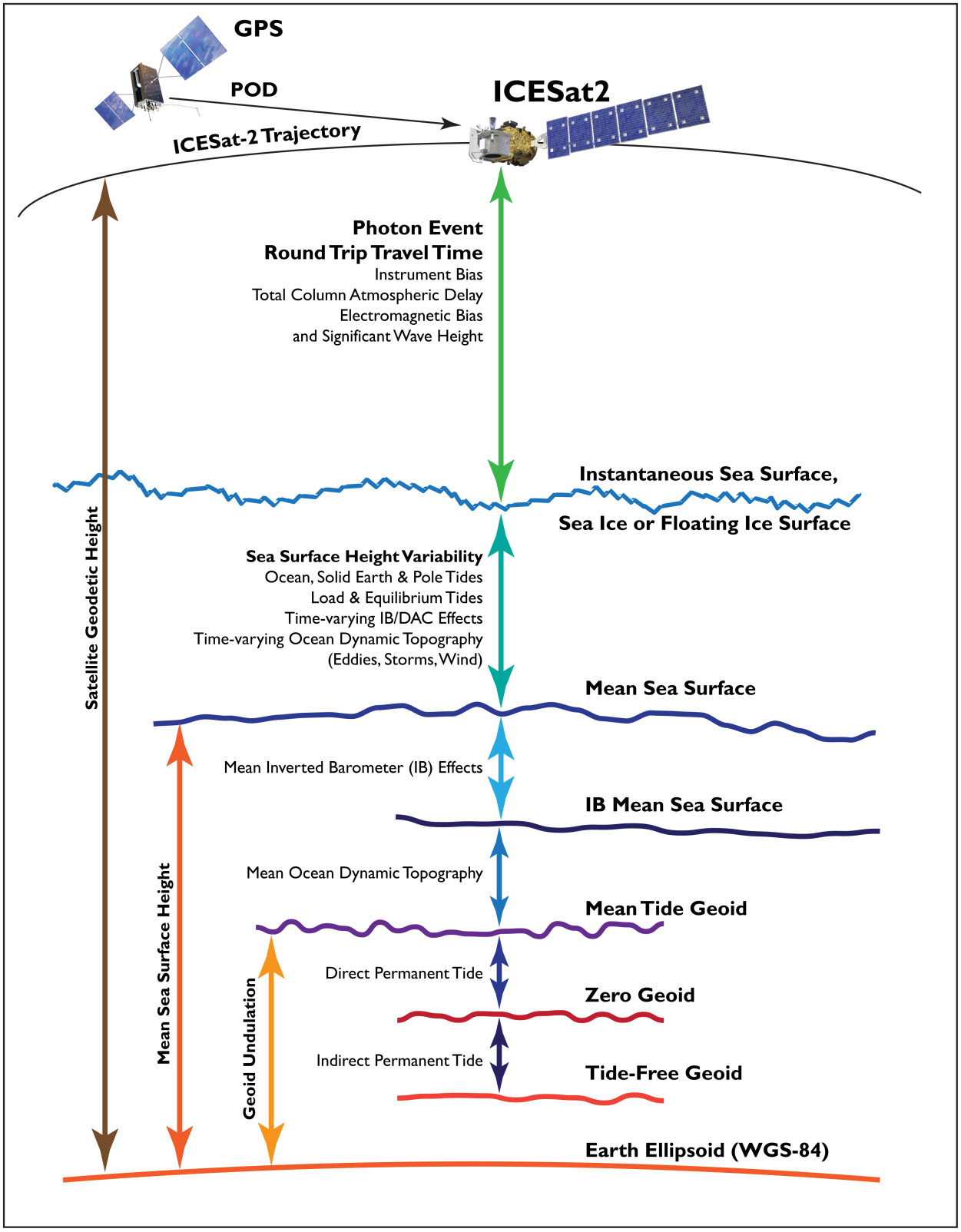

Modified from: Tapley, B. D. & M-C. Kim, Applications to Geodesy, Chapt. 10 in *Satellite Altimetry and Earth Sciences*, ed. by L-L. Fu & A. Cazenave, Academic Press, pp. 371-406, 2001.

Figure 5.1: Schematic of geophysical corrections utilized in satellite altimetry

5.1 Ocean Tide Corrections (including Long-Period Ocean Tides)

The ocean tides and long-period tides are not applied to the photon heights on ATL03 and are provided only as reference values at the geolocation segment rate. Higher level products may (or may not) have applied these values (see Table 5.1).

Ocean tides account for about 70% of the total variability of the ocean surface at daily and half-daily periods (diurnal and semi-diurnal). The effects of tides vary regionally; open ocean areas typically have smaller amplitudes ($\pm$0.3 m r.m.s) than continental shelves and coastal regions (which can increase to several meters, or more). In shallow seas, interactions with the sea floor can cause non-linear interactions between tidal constituents and generate amplitudes at new frequencies (resulting in compound tides and overtides).

Ocean tide models quantitatively describe the time-variant changes of sea level due to gravitational attraction by the sun and moon. Global tide models are applicable for any point in the oceans, as well as on sea ice and under the peripheral ice shelves of Antarctica and Greenland.

Beginning with Release 007, ocean tide values are computed from the `FES2014b` extrapolated ocean tide model, with 27 short-period tidal constituents computed via a modified version of `perth5.f` Fortran routines. These constituents include: $K1$, $M2$, $N2$, $O1$, $P1$, $Q1$, $S1$, $S2$, $K2$, $2N2$, $EPS2$, $J1$, $L2$, $T2$, $La2$, $Mu2$, $Nu2$, $R2$, $M3$, $M4$, $M6$, $M8$, $MKS2$, $MN4$, $MS4$, $N4$, and $S4$ (c.f. Figure 5.2). Six long-period tidal constituents are computed by a modified version of `perth_lp.f` Fortran routines. These constituents include: MSf, Mf, Mm, $MSqm$, Mtm, and Ssa. The Sa constituent was purposefully omitted due to having been identified as suspect (Richard Ray, private communication). Both sets of Fortran routines were originally authored by Richard Ray and are openly available.

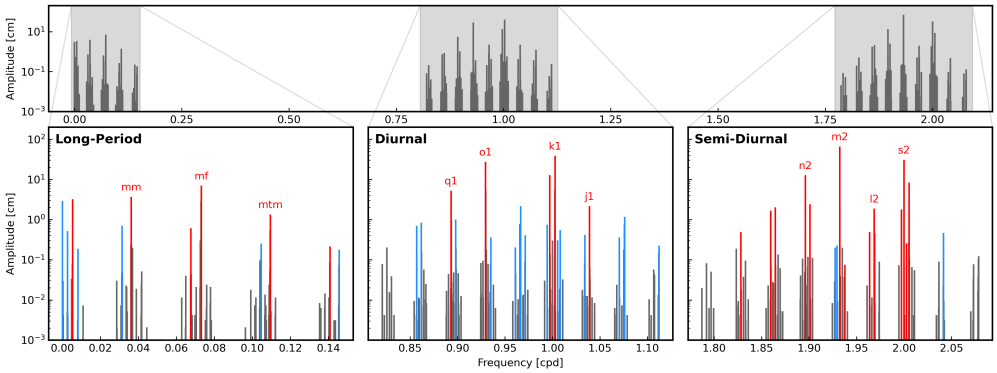

Figure 5.2: Frequencies and equilibrium amplitudes of semi-diurnal, diurnal and long-period tides from Cartwright and Tayler [1971]. Red spectral lines are constituents included in the `FES2014b` model, and blue spectral lines are constituents inferred using the `perth5` routines from Richard Ray (GSFC).

The computations for short-period ocean tide reference values, as well as long-period tides are performed by computing a modeled tidal height at each reference photon ($\sim$20 meters, along-track) latitude and longitude, along with its corresponding time, t. For locations where the ocean tide is undefined (e.g., over land), the value of the ocean tide correction is set to an invalid value (approximately 3.4E38).

Parameters for the short and long-period ocean tides are found in ATL03 as `gtx/geophys_corr/tide_ocean` and `gtx/geophys_corr/tide_equilibrium` respectively. Prior to Release 007, the long-period tides were calculated assuming an "equilibrium response", where the ocean freely responds to the tidal forces without the influence of inertia, currents or the irregular distribution of land [Cartwright and Tayler, 1971; Proudman, 1960]. For Release 007, the long-period constituents are provided by `FES2014b` or inferred, and so the equilibrium moniker is largely historical.

5.1.1 `FES2014b` (Extrapolated) Ocean Tide Model

There are some nuances in the extrapolated version of `FES2014b` ocean tides that some ICESat-2 data users should be aware of. The model was developed to provide tidal predictions in the open ocean and to provide an estimate of ocean tides in near-coastal and shallow-sea regions, including estuaries, inlets and fjords. The resolution of the `FES2014b` model is $1/16°$, and, in extrapolated form, it can provide ocean tide predictions in areas located well inland of neighboring shores. Users are cautioned to ignore over-land values, and to understand that small-scale modeling in estuaries, inlets and fjords are of diminished quality when compared to open-ocean tidal predictions.

A root sum square standard deviation difference analysis of seven data-constrained ocean tide models [Stammer et al., 2014] indicated regions with ocean depths <1000m have lower consistency (higher variance) across the models than regions with ocean depths >1000m, at a level of being up to six times higher. Figure 1 of Stammer et al. [2014], shows that the highest variance between all seven models ($M1$ and $K1$ constituents) takes place in regions including the Arctic (∼75° N), a latitude band surrounding Antarctica (75° S), along the northern coast of Australia, through the East Indies, and along the coasts of East Asia.

Detailed Examples of Tide Model Edges: Figure 5.3 shows examples of ocean tide evaluations for 5°×5° regions, computed at 1 arc-minute resolution, displaying how the extrapolated `FES2014b` model extends tidal predictions inland of coastal edges. Figure 5.4 show (a) the Southern Ocean and peripheral ice shelves of Antarctica; and (b) the Arctic ocean in polar stereographic maps.

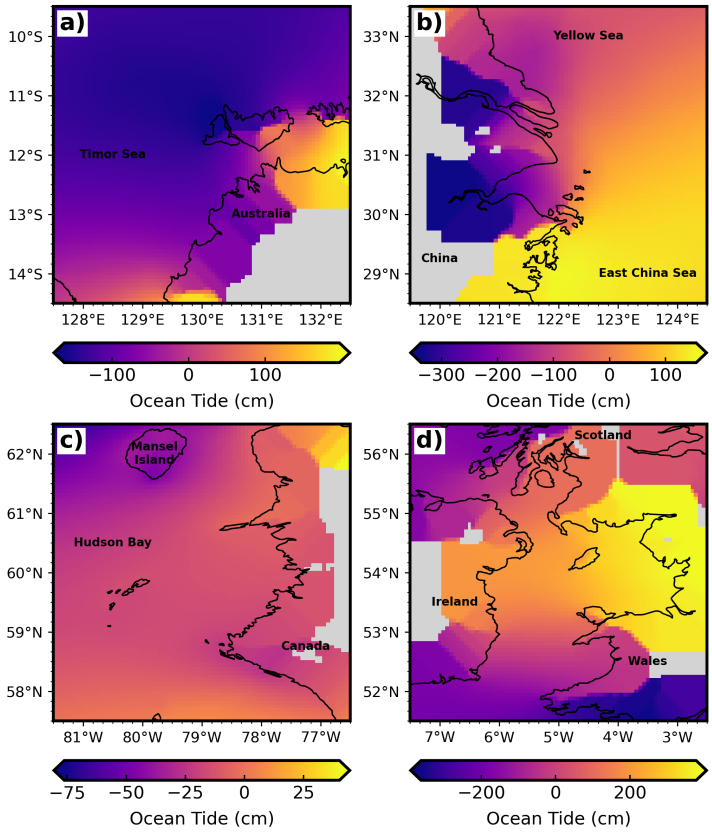

Figure 5.3: 5°×5° examples of extrapolated `FES2014b` ocean tidal fields computed for June 4, 2019 at 12:00:00Z for (a) off the coast of NW Australia; (b) China coast, near Shanghai; (c) Northeast coast of Hudson Bay, Canada; and (d) the Irish Sea.

Figure 5.3a shows a region off the NW coast of Australia, possessing a fairly large tidal gradient running from -162 cm (NW of Melville Island) and growing to 198 cm towards the east. Gray zones are where the constituent grids are masked to prevent a valid estimate of the ocean tide. Figure 5.3b shows a region near Shanghai, China. Low tides are seen along the Yellow Sea coast, and high tides for inlets south of Hangzhou Bay. Figure 5.3c shows, at this moment in time, a relatively low dynamic tidal region in northeast Hudson Bay, Canada. Figure 5.3d shows tides in the Irish Sea varying from -3 to 3 meters along the south and north coasts of Wales, respectively.

Maps found in Figure 5.3 and Figure 5.4 clearly demonstrate that ocean tide predictions extend well inland and for Antarctica well beyond the ice sheet grounding zone. Users must be aware of and proceed with caution when making studies in such regions. Only nearshore lakes and enclosed seas are zeroed out in the extrapolated `FES2014b` solution. Application of a detailed shoreline mask must be applied to prevent inadvertently applying ocean tide values as a correction for other locations. For Antarctic grounding zones, the ice surface response to ocean forcing is generally dampened relative to its hydrostatic value [Padman et al., 2018]. Users should again proceed with caution as using the extrapolated `FES2014b` tides directly could lead to an "over-correction".

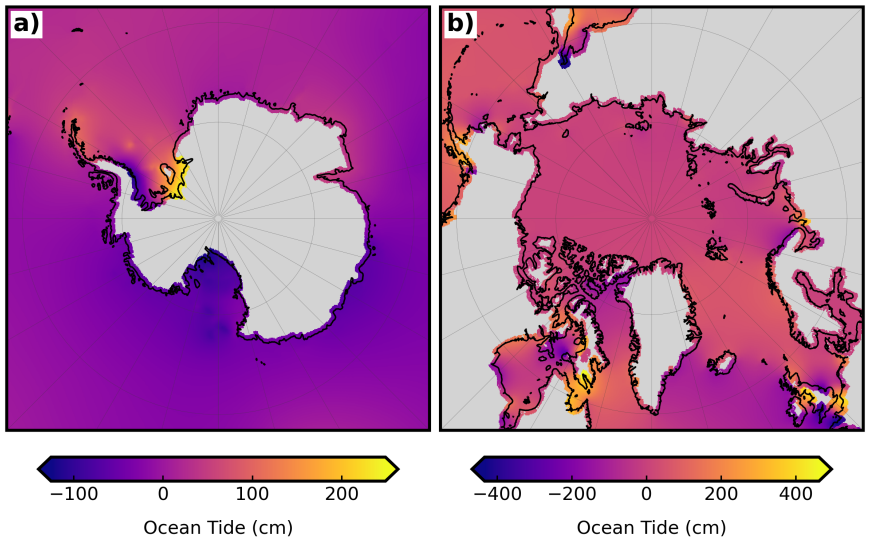

Figure 5.4: 10km examples of extrapolated `FES2014b` ocean tidal fields computed for June 4, 2019 at 12:00:00Z for (a) Southern Ocean and Antarctic ice shelves; (b) Arctic Ocean and North Atlantic.

5.2 Ocean Loading Correction

This correction accounts for the deformation of the Earth's crust due to the weight of overlying ocean tides. As the tides rise and fall, mass is added or lost in the water column and this mass redistribution causes loading of the ocean bottom [Agnew, 2015].

Ancillary ocean loading phase and amplitude files corresponding to the `FES2014b` ocean tide model provide the basis for computing corrections for ocean loading for ICESat-2. All 27 short-period and six long-period constituents from `FES2014b` (excluding Sa) are utilized (list given in Section 5.1).

For each reference photon (∼20 meters, along-track), based on its location (latitude, longitude) and corresponding time, ocean load induced vertical displacements are computed. This value has been subtracted for all photon heights on ATL03. The parameter is found on ATL03 in `gtx/geophys_corr/tide_load`.

5.3 Solid Earth Tide Correction

The correction for solid earth tides considers the deformation (elastic response) of the solid earth (including the sea floor) due to the attractions of the Sun and Moon. Ninety-five percent of the tidal energy comes from the second-degree tides. The procedures adopted by the ICESat-2 mission for the calculation of solid earth tide displacements follows those recommended by the IERS Conventions 2010 [Petit and Luzum, 2010].

A two-step process was followed by ATL03 for computing the solid earth tides: (1) calculate displacements utilizing nominal (frequency-independent) values of the Love and Shida numbers for the second and third degree harmonics of the tidal potential; (2) compute further corrections to account for the frequency-dependent deviations of the Love and Shida numbers [Figure 5.5], and the variations arising from mantle anelasticity [Mathews et al., 1997; Wahr, 1981]. When compared in the same tide system, the RMS difference between the rigorous IERS model used by ICESat-2 and the simpler models used by other altimetry missions is typically less than 2 mm [Ray, 2013].

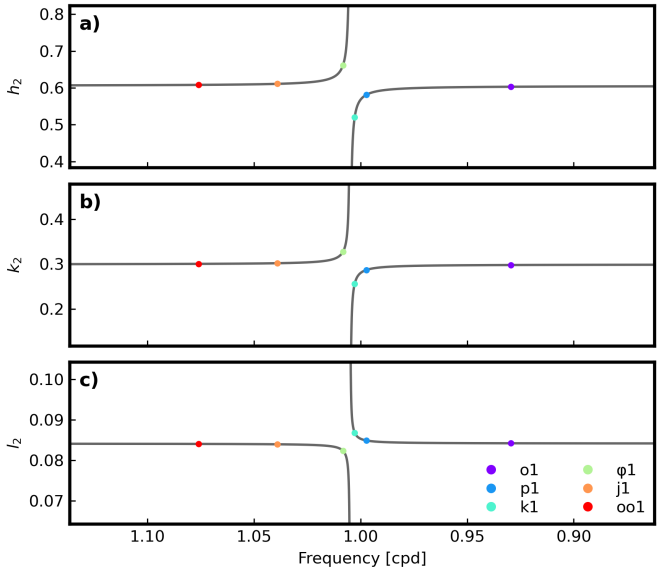

Figure 5.5: Frequency dependence of Love and Shida Numbers from Wahr [1981]

As described in Section 2.3, the solid earth tides reported on ATL03 are provided to produce heights in the tide free system [Table 5.2]. The solid earth tide parameter is found on ATL03 in `gtx/geophys_corr/tide_earth`. The conversion term needed to transform values from the tide free system into mean tide system is provided by the `tide_earth_free2mean` parameter.

Table 5.2: Solid earth tide specifications by mission

Mission	Formalism	Tidal System
ICESat-2	Petit and Luzum [2010]	Tide Free
SWOT	Cartwright and Edden [1973]	Mean Tide
ICESat (GLAS)	Cartwright and Edden [1973]	Mean Tide
CryoSat-2	Cartwright and Edden [1973]	Mean Tide

5.4 Solid Earth and Ocean Pole Tide Correction

The Earth's rotation axis is inclined at an angle of 23.5 degrees to the celestial pole, and rotates about it once every 26,000 years [Kantha and Clayson, 2000]. Superimposed on this long-term precession, the rotation axis of the Earth shifts with respect to its mean pole location due to nutation, Chandler wobble, annual variations, and other processes [Desai, 2002; Wahr, 1985]. Load and ocean pole tides are driven by these variations, the corresponding elastic response, and for the case of ocean pole tides the centripetal effects of polar motion on the ocean [Desai et al., 2015]. The process utilized by ATL03 calculates the pole tide displacements in the radial direction using daily polar motion values (x_p, y_p) and Love number values appropriate to the frequency of the pole tide (c.f., eq. 7.26 in Petit and Luzum [2010]). For Release 007, ATL03 uses the "secular pole" model (x_s and y_s) as the terrestrial reference for calculating deflections in pole position [2018 update to Petit and Luzum, 2010].

$$x_s(t) = 0.055 + 0.001677(t - 2000.0)$$
$$y_s(t) = 0.3205 + 0.00346(t - 2000.0)$$

The solid earth pole tide parameter is found on ATL03 in `gtx/geophys_corr/tide_pole`, and the ocean pole tide parameter is found in `gtx/geophys_corr/tide_oc_pole`.

5.5 Inverted Barometer (IB) Correction and Dynamic Atmospheric Correction (DAC)

The Dynamic Atmospheric Correction (DAC) is not applied to the photon heights on ATL03 and is provided only as reference values at the geolocation segment rate (see Table 5.1).

These two corrections, IB and DAC are inter-related, conceptually. The IB correction describes the response of the ocean's surface level caused by variations in atmospheric pressure (i.e., high and low pressure systems) [Wunsch and Stammer, 1997]. The DAC correction contains IB as well as water mass momentum forcing driven by the highly variable wind stress field. In the most general sense, DAC provides a much more dynamic surface response than IB.

ATL03 provides reference values from the MOG2D DAC (2 Dimensions Gravity Waves model). This DAC is provided courtesy of AVISO and is available in six-hour increments, at a 0.25° geographic resolution. The ATL03 algorithm computes values along-track every ~20 m, which have been simultaneously interpolated, both geographically and temporally. The parameter is found on ATL03 in `gtx/geophys_corr/dac`.

On the sea ice height product (ATL07), both the DAC and IB are provided as variables. Starting with Release 007, the DAC is applied at the segment output rate. Previous releases of ATL07 used IB, which was derived from the sea level pressure data provided by the ATL09 atmospheric product [Kwok et al., 2023]. The IB parameter is found on ATL07 in `gtx/sea_ice_segments/geophysical/height_segment_ib`, and the DAC parameter is found in `gtx/sea_ice_segments/geophysical/height_segment_dac`.

Release 006 (and earlier) comparisons of ATL07 with ATL12 (upper-level ocean product) can introduce a situation whereby ATL07 had the IB correction applied, and ATL12 had the DAC applied. These two corrections had to be reconciled before attempting to make comparisons. Starting with Release 007, both ATL07 and ATL12 have applied the DAC to their respective heights.

References

D. C. Agnew. *Earth Tides*, pages 151–178. Elsevier, 2015. doi: 10.1016/B978-0-444-53802-4.00058-0. https://doi.org/10.1016/b978-0-444-53802-4.00058-0.

D. E. Cartwright and A. C. Edden. Corrected Tables of Tidal Harmonics. *Geophysical Journal of the Royal Astronomical Society*, 33(3):253–264, 1973. ISSN 0956-540X. doi: 10.1111/j.1365-246X.1973.tb03420.x. https://doi.org/10.1111/j.1365-246X.1973.tb03420.x.

D. E. Cartwright and R. J. Tayler. New Computations of the Tide-generating Potential. *Geophysical Journal of the Royal Astronomical Society*, 23(1):45–73, 1971. ISSN 0956-540X. doi: 10.1111/j.1365-246X.1971.tb01803.x. https://doi.org/10.1111/j.1365-246X.1971.tb01803.x.

S. Desai. Observing the pole tide with satellite altimetry. *Journal of Geophysical Research: Oceans*, 107 (C11), 2002. ISSN 0148-0227. doi: 10.1029/2001JC001224. https://doi.org/10.1029/2001jc001224.

S. Desai, J. Wahr, and B. Beckley. Revisiting the pole tide for and from satellite altimetry. *Journal of Geodesy*, 89(12):1233–1243, 2015. ISSN 0949-7714. doi: 10.1007/s00190-015-0848-7. https://doi.org/10.1007/s00190-015-0848-7.

B. Hofmann-Wellenhof and H. Moritz. *Physical Geodesy*. Springer Vienna, 2006. ISBN 9783211335444. doi: 10.1007/978-3-211-33545-1. https://doi.org/10.1007/978-3-211-33545-1.

L. H. Kantha and C. A. Clayson. *Numerical models of oceans and oceanic processes*, volume 66. Academic Press, San Diego, CA, 2000. ISBN 0124340687. doi: 10.1016/s0074-6142(00)x8001-1. https://doi.org/10.1016/s0074-6142(00)x8001-1.

R. Kwok and J. Morison. Sea surface height and dynamic topography of the ice-covered oceans from CryoSat-2: 2011–2014. *Journal of Geophysical Research: Oceans*, 121(1):674–692, 2016. ISSN 2169-9275. doi: 10.1002/2015JC011357. https://doi.org/10.1002/2015jc011357.

R. Kwok, A. Petty, M. Bagnardi, J. T. Wimert, G. F. Cunningham, D. W. Hancock, A. Ivanoff, and N. Kurtz. *Ice, Cloud, and Land Elevation Satellite (ICESat-2) Project Algorithm Theoretical Basis Document (ATBD) for Sea Ice Products*. NASA Goddard Space Flight Center, 2023. doi: 10.5067/9VT7NJWOTV3I. https://doi.org/10.5067/9VT7NJWOTV3I. Release 006.

J. Mäkinen and J. Ihde. The Permanent Tide In Height Systems. In M. G. Sideris, editor, *Observing our Changing Earth*, pages 81–87, Berlin, Heidelberg, 2009. Springer Berlin Heidelberg. ISBN 978-3-540-85426-5. doi: 10.1007/978-3-540-85426-5_10. https://doi.org/10.1007/978-3-540-85426-5_10.

P. M. Mathews, V. Dehant, and J. M. Gipson. Tidal station displacements. *Journal of Geophysical Research: Solid Earth*, 102(B9):20469–20477, 1997. ISSN 0148-0227. doi: 10.1029/97JB01515. https://doi.org/10.1029/97jb01515.

T. A. Neumann, A. J. Martino, T. Markus, S. Bae, M. R. Bock, A. C. Brenner, K. M. Brunt, J. Cavanaugh, S. T. Fernandes, D. W. Hancock, K. Harbeck, J. Lee, N. T. Kurtz, P. J. Luers, S. B. Luthcke, L. Magruder, T. A. Pennington, L. Ramos-Izquierdo, T. Rebold, J. Skoog, and T. C. Thomas. The Ice, Cloud, and Land Elevation Satellite – 2 mission: A global geolocated photon product derived from the Advanced Topographic Laser Altimeter System. *Remote Sensing of Environment*, 233:111325, 2019. ISSN 0034-4257. doi: 10.1016/j.rse.2019.111325. https://doi.org/10.1016/j.rse.2019.111325.

L. Padman, M. R. Siegfried, and H. A. Fricker. Ocean Tide Influences on the Antarctic and Greenland Ice Sheets. *Reviews of Geophysics*, 56(1):142–184, 2018. ISSN 8755-1209. doi: 10.1002/2016RG000546. https://doi.org/10.1002/2016rg000546.

G. Petit and B. Luzum. IERS Conventions (2010). Technical Report 36, Bureau International des Poids et Mesures (BIPM), US Naval Observatory (USNO), 2010. http://www.iers.org/nn_11216/IERS/EN/Publications/TechnicalNotes/tn36.html.

J. Proudman. The Condition that a Long-Period Tide shall follow the Equilibrium-Law. *Geophysical Journal International*, 3(2):244–249, 1960. ISSN 0956-540X. doi: 10.1111/j.1365-246X.1960.tb00392.x. https://doi.org/10.1111/j.1365-246x.1960.tb00392.x.

R. H. Rapp, R. S. Nerem, C. K. Shum, S. M. Klosko, and R. G. Williamson. Consideration of permanent tidal deformation in the orbit determination and data analysis for the Topex/Poseidon mission. Technical Report NASA-TM-100775, NASA Goddard Space Flight Center, 1991. https://ntrs.nasa.gov/citations/19910021305.

R. D. Ray. Precise comparisons of bottom-pressure and altimetric ocean tides. *Journal of Geophysical Research: Oceans*, 118(9):4570–4584, 2013. ISSN 2169-9275. doi: 10.1002/jgrc.20336. https://doi.org/10.1002/jgrc.20336.

J. Robbins, T. Sutterley, T. Neumann, N. Kurtz, M. Bagnardi, K. Brunt, A. Gibbons, D. Hancock, J. Lee, and S. Luthcke. *ICESat-2 Data Comparison Guide for Release 007*. ICESat-2 Project, 2025. doi: 10.5281/zenodo.16389971. https://doi.org/10.5281/zenodo.16389971.

B. E. Schutz and T. J. Urban. The GLAS Algorithm Technical Basis Document for Laser Footprint Location (Geolocation) and Surface Profiles. Technical Report TM-2014-208641, NASA Goddard Space Flight Center, Greenbelt, Maryland USA, 2014. https://ntrs.nasa.gov/citations/20140017859.

D. Stammer, R. D. Ray, O. B. Andersen, B. K. Arbic, W. Bosch, L. Carrère, Y. Cheng, D. S. Chinn, B. D. Dushaw, G. D. Egbert, S. Y. Erofeeva, H. S. Fok, J. A. M. Green, S. Griffiths, M. A. King, V. Lapin, F. G. Lemoine, S. B. Luthcke, F. Lyard, J. Morison, M. Müller, L. Padman, J. G. Richman, J. F. Shriver, C. K. Shum, E. Taguchi, and Y. Yi. Accuracy assessment of global barotropic ocean tide models. *Reviews of Geophysics*, 52(3):243–282, 2014. ISSN 1944-9208. doi: 10.1002/2014RG000450. https://doi.org/10.1002/2014RG000450.

J. M. Wahr. Body tides on an elliptical, rotating, elastic and oceanless Earth. *Geophysical Journal of the Royal Astronomical Society*, 64(3):677–703, 1981. ISSN 1365-246X. doi: 10.1111/j.1365-246X.1981.tb02690.x. https://doi.org/10.1111/j.1365-246X.1981.tb02690.x.

J. M. Wahr. Deformation induced by polar motion. *Journal of Geophysical Research: Solid Earth*, 90 (B11):9363–9368, 1985. ISSN 0148-0227. doi: 10.1029/JB090iB11p09363. https://doi.org/10.1029/jb090ib11p09363.

C. Wunsch and D. Stammer. Atmospheric loading and the oceanic "inverted barometer" effect. *Reviews of Geophysics*, 35(1):79–107, 1997. ISSN 8755-1209. doi: 10.1029/96RG03037. https://doi.org/10.1029/96rg03037.

A Glossary

Ellipsoid: a mathematical construct, flattened at the poles, suitable for unequivocally describing horizontal and vertical positions. Ellipsoids are typically defined by two parameters: the semi-major axis (a) and the amount of flattening (f), typically described by its inverse, $1/f$.

Equipotential Surface: a surface of constant potential energy, where the gravitational force is perpendicular to the surface at all points. The *geoid* is an example of an equipotential surface, representing mean sea level in the absence of tides and other disturbances.

Flattening: describes the extent of rotational ellipsoid axial difference, defined by $f = (a-b)/a$, where a is the semi-major (equatorial) axis and b is the semi-minor (polar) axis.

Geoid: a level, or equipotential surface of the Earth's gravity field corresponding to sea level (free of ocean currents and other disturbances; such as ocean tides, barometric and wind effects, etc.).

Geophysical Corrections: a grouping of temporal (time-varying) processes, originating gravitationally or by other forcing sources, that are modeled to such accuracy that they can be used to correct a range measurement for a variety of dynamic effects.

Love Numbers: unitless ratios that provide a measure of rigidity of a planetary body and the susceptibility of its shape to change in response to a tidal potential. The Love number, h, is the ratio of the elastic radial displacement of a mass element of the actual Earth to the radial displacement of the corresponding hypothetical fluid Earth, or, to put it another way, the height of the body tide to the height of the equilibrium (static) marine tide. The Love number, k, is the ratio of the additional potential produced by the redistribution of mass to the deforming potential.

Mean Tide System: the permanent tide is included in defining the shape of the Earth. The shape therefore corresponds to the long-time average under lunar- and solar-tidal forcing.

Radius of Curvature: on an ellipsoid, two mutually perpendicular normal sections whose curvatures are minimum and maximum. These are termed the principle normal sections: meridian (M); and prime vertical (N). Generally, $N \geq M$; however at the poles ($\varphi = \pm 90°$), $M_{90°} = N_{90°} = a^2/b$; and at the equator ($\varphi = 0$), $M_{0°} = b^2/a$ and $N_{0°} = a$.

Range: generally, half of the observed travel time (Dt) a signal takes to traverse the distance between an on-board emitter (laser or radar), a reflection point, and an on-board receiver, scaled by the speed of light (c). Range $= c(Dt/2)$, neglecting path delays.

Tide Free System: the permanent tide is eliminated from the shape of the Earth. From the potential field quantities (gravity, geoid, etc.) both the tide-generating potential, and the deformation potential of the Earth (the indirect effect) are eliminated. This corresponds to physically removing the Sun and the Moon to infinity.

Zero Tide System: eliminates the tide-generating potential but retains its indirect effect, i.e., the potential of the permanent deformation of the Earth.

B ITRF2020 Transformation Parameters

Source: https://itrf.ign.fr/docs/solutions/itrf2020/Transfo-ITRF2020_TRFs.txt
Transformation parameter calculator: https://itrf.ign.fr/en/solutions/transformations

Transformation parameters from ITRF2020 to past ITRFs.

SOLUTION	Tx	Ty	Tz	D	Rx	Ry	Rz	EPOCH
UNITS---------->	mm	mm	mm	ppb	.001"	.001"	.001"	
	.	.	.	.	.	.	.	
RATES	Tx	Ty	Tz	D	Rx	Ry	Rz	
UNITS---------->	mm/y	mm/y	mm/y	ppb/y	.001"/y	.001"/y	.001"/y	
ITRF2014	-1.4	-0.9	1.4	-0.42	0.00	0.00	0.00	2015.0
rates	0.0	-0.1	0.2	0.00	0.00	0.00	0.00	
ITRF2008	0.2	1.0	3.3	-0.29	0.00	0.00	0.00	2015.0
rates	0.0	-0.1	0.1	0.03	0.00	0.00	0.00	
ITRF2005	2.7	0.1	-1.4	0.65	0.00	0.00	0.00	2015.0
rates	0.3	-0.1	0.1	0.03	0.00	0.00	0.00	
ITRF2000	-0.2	0.8	-34.2	2.25	0.00	0.00	0.00	2015.0
rates	0.1	0.0	-1.7	0.11	0.00	0.00	0.00	
ITRF97	6.5	-3.9	-77.9	3.98	0.00	0.00	0.36	2015.0
rates	0.1	-0.6	-3.1	0.12	0.00	0.00	0.02	
ITRF96	6.5	-3.9	-77.9	3.98	0.00	0.00	0.36	2015.0
rates	0.1	-0.6	-3.1	0.12	0.00	0.00	0.02	
ITRF94	6.5	-3.9	-77.9	3.98	0.00	0.00	0.36	2015.0
rates	0.1	-0.6	-3.1	0.12	0.00	0.00	0.02	
ITRF93	-65.8	1.9	-71.3	4.47	-3.36	-4.33	0.75	2015.0
rates	-2.8	-0.2	-2.3	0.12	-0.11	-0.19	0.07	
ITRF92	14.5	-1.9	-85.9	3.27	0.00	0.00	0.36	2015.0
rates	0.1	-0.6	-3.1	0.12	0.00	0.00	0.02	
ITRF91	26.5	12.1	-91.9	4.67	0.00	0.00	0.36	2015.0
rates	0.1	-0.6	-3.1	0.12	0.00	0.00	0.02	
ITRF90	24.5	8.1	-107.9	4.97	0.00	0.00	0.36	2015.0
rates	0.1	-0.6	-3.1	0.12	0.00	0.00	0.02	
ITRF89	29.5	32.1	-145.9	8.37	0.00	0.00	0.36	2015.0
rates	0.1	-0.6	-3.1	0.12	0.00	0.00	0.02	
ITRF88	24.5	-3.9	-169.9	11.47	0.10	0.00	0.36	2015.0
rates	0.1	-0.6	-3.1	0.12	0.00	0.00	0.02	

Note : These parameters are derived from those already published in the IERS Technical Notes and Annual Reports, and from the transformation parameters between ITRF2020, ITRF2014 and ITRF2008. They supersede all values published in the past IERS/ITRF documentations. The transformation parameters should be used with the standard model (1) given below and are valid at the indicated epoch.

```
: XS :    : X :   : Tx :   :  D   -Rz   Ry : : X :
:    :    :   :   :    :   :               : :   :
: YS :  = : Y : + : Ty : + :  Rz   D   -Rx : : Y :                    (1)
:    :    :   :   :    :   :               : :   :
: ZS :    : Z :   : Tz :   : -Ry   Rx   D  : : Z :
```

Where X,Y,Z are the coordinates in ITRF2020 and XS,YS,ZS are the coordinates in the other frames.

On the other hand, for a given parameter P, its value at any epoch t is obtained by using equation (2).

$$P(t) = P(EPOCH) + \dot{P} * (t - EPOCH) \qquad (2)$$

where EPOCH is the epoch indicated in the above table (currently 2015.0)
and $\dot{P}$ is the rate of that parameter.

C PROJ Pipelines

PROJ is an open source library for performing *Coordinate Reference System* (CRS) transformations. In Python, the `pyproj` and `geopandas` libraries provide interfaces to PROJ. The following code snippets provide the PROJ4 pipelines for transforming between the reference frames used by ICESat-2, SWOT, CryoSat-2 and ICESat (GLAS). These pipelines use the two-step transformation procedure outlined in Section 3.1.1 and Section 3.2, and use the *Helmert* parameter values from Appendix B. These `pyproj` transform functions take longitude (λ, degrees), latitude (φ, degrees), height (h, meters) and time (t, years) as inputs, and return the transformed coordinates in the same units.

Transformation from TOPEX/Poseidon (ITRF2008) to WGS84 (ITRF2014):

```
# TOPEX/Poseidon Ellipsoid in ITRF2008 to WGS84 Ellipsoid in ITRF2020
pipeline = """+proj=pipeline
    +step +proj=unitconvert +xy_in=deg +z_in=m +xy_out=rad +z_out=m
    +step +proj=cart +a=6378136.3 +rf=298.257
    +step +proj=helmert +x=-0.0016 +y=-0.0019 +z=-0.0024 +rx=0 +ry=0 +rz=0 +s=2e-05
        +dx=0 +dy=0 +dz=0.0001 +drx=0 +dry=0 +drz=0 +ds=-3e-05
        +t_epoch=2010 +convention=position_vector
    +step +inv +proj=cart +ellps=WGS84
    +step +proj=unitconvert +xy_in=rad +z_in=m +xy_out=deg +z_out=m"""
transformer = pyproj.Transformer.from_pipeline(pipeline)
```

Transformation from TOPEX/Poseidon (ITRF2008) to WGS84 (ITRF2020)

```
# TOPEX/Poseidon Ellipsoid in ITRF2008 to WGS84 Ellipsoid in ITRF2020
pipeline = """+proj=pipeline
    +step +proj=unitconvert +xy_in=deg +z_in=m +xy_out=rad +z_out=m
    +step +proj=cart +a=6378136.3 +rf=298.257
    +step +proj=helmert +x=-0.0002 +y=-0.001 +z=-0.0033 +rx=0 +ry=0 +rz=0 +s=0.00029
        +dx=0 +dy=0.0001 +dz=-0.0001 +drx=0 +dry=0 +drz=0 +ds=-3e-05
        +t_epoch=2015 +convention=position_vector
    +step +inv +proj=cart +ellps=WGS84
    +step +proj=unitconvert +xy_in=rad +z_in=m +xy_out=deg +z_out=m"""
transformer = pyproj.Transformer.from_pipeline(pipeline)
```

Transformation from WGS84 (ITRF2014) to WGS84 (ITRF2020)

```
# WGS84 Ellipsoid in ITRF2014 to WGS84 Ellipsoid in ITRF2020
pipeline = """+proj=pipeline
    +step +proj=unitconvert +xy_in=deg +z_in=m +xy_out=rad +z_out=m
    +step +proj=cart +ellps=WGS84
    +step +proj=helmert +x=0.0014 +y=0.0009 +z=-0.0014 +rx=0 +ry=0 +rz=0 +s=0.00042
        +dx=0 +dy=0.0001 +dz=-0.0002 +drx=0 +dry=0 +drz=0 +ds=0
        +t_epoch=2015 +convention=position_vector
    +step +inv +proj=cart +ellps=WGS84
    +step +proj=unitconvert +xy_in=rad +z_in=m +xy_out=deg +z_out=m"""
transformer = pyproj.Transformer.from_pipeline(pipeline)
```

Coordinate Reference System Transform

Using the coordinate and height values from the ITRF transformation example and the TOPEX/Poseidon (ITRF2008) to WGS84 (ITRF2020) pipeline, we can transform the coordinates as follows:

```
lon, lat, h, t = transformer.transform(10, 42, 210, 2005.3)
```

This results in longitude, latitude and height values of $9°59'59.9995''$, $41°59'59.9999''$, and 209.2956m respectively, which matches the results from our example.